Imaging of a Thin Oxide Film Formation from the Combination of Surface Reflectivity and Electrochemical Methods.

Sara Chakri, Anisha N Patel, Isabelle Frateur, Frédéric Kanoufi, Eliane Sutter, Mai Tran Tron Long, Bernard Tribollet, Vincent Vivier

▶ **To cite this version:**

HAL Id: hal-01523907

https://hal.sorbonne-universite.fr/hal-01523907v1

Submitted on 3 Feb 2023

Imaging of a corroding surface from the combination of surface reflectivity and electrochemical methods

S. Chakri,[1] A.N. Patel,[2] I. Frateur,[1] F. Kanoufi,[2,*] E. Sutter,[1]
T.T.M. Tran,[1] B. Tribollet,[1] V. Vivier[1,*]

1- Sorbonne Universités, UPMC Univ Paris 06, CNRS, Laboratoire Interfaces et Systèmes Electrochimiques, 4 place Jussieu, F-75005, Paris, France
2- Sorbonne Paris Cité, Paris Diderot University, Interfaces, Traitements, Organisation et Dynamique des Systèmes Laboratory, CNRS-UMR 7086, 15 rue J. A. Baif, 75013 Paris, France

*e-mails: vincent.vivier@upmc.fr; frederic.kanoufi@univ-paris-diderot.fr

Abstract

Electrochemical methods (cyclic voltammetry (CV), potential steps, and electrochemical impedance spectroscopy), were successfully combined with *in situ* reflectometry measurements for a detailed analysis of the passive layer evolution as a function of the electrode potential. Interestingly, both EIS and surface reflectivity allowed a film thickness in the nanometer range to be readily determined. In addition, transient analyses of the reflectivity simultaneously recorded with CVs show the formation of both Fe_2O_3 and Fe_3O_4 oxides. The image analysis showed that the steel surface reactivity is heterogeneous and presents micrometric islands coated with thicker oxide layer than the surrounding surface. The *in situ* combination of these techniques thus offers a powerful analytical description of the interface on local scale and its transient response to a perturbation.

Keywords: *Reflectometry, Electrochemical impedance spectroscopy, Cyclic voltammetry, Local reactivity, Passive layer*

1. Introduction

Electrochemistry inherently shows heterogeneity: importance of edge effects at electrodes,[1] or defects[2] where higher current densities are observed; this can have dramatic effects as illustrated in our daily life in corrosion. However, electrochemical current is an average response of the electrochemical process while local information has considerable importance. In this respect, different electrochemical imaging techniques have been developed to access such local electrochemical information. Scanning electrochemical microscopy (SECM) is the most popular,[3] and was used to identify, to some extent, pitting/corroding sites from materials (Ta,[4] Ti,[5] or Mg[6]). It can also be operated as a local impedance imaging/measurement tool.[7] However, a major drawback for a time-evolving system is the low image acquisition frequency for scanning probe techniques, and image resolution, although the recent development of scanning electrochemical cell microscope (SECCM) and nanoprobes have brought considerable improvement,[8] compatibility with the timescale of the corrosion of most materials is still an issue.

Optical microscopies (ellipsometry[9] or light absorption)[10] offer a promising means to study *in situ* the growth and transformation of passive oxide films on metals.[11] If their coupling with electrochemistry has been practiced since the early 1980s, it is only very recently that optical microscopes were developed allowing much faster image acquisition with sub-micrometer resolution. For instance Tao *et al.*[12] have developed the coupling of Surface Plasmon Resonance (SPR) imaging for monitoring the local change in refractive index in the vicinity of a SPR active surface (typically a thin Au layer electrode). Other opto-electrochemical approaches have been proposed[13] using local refractive index imaging but with possible transposition to any kind of material, not solely SPR-dedicated thin and transparent electrodes. In such opto-electrochemical microscopies, a local electrochemical current (or chemical flux) is inferred from the changes in optical signal (SPR intensity, light polarization

for ellipsometry, reflected light intensity…) recorded by a CCD camera. We propose herein the imaging of corrosion processes by a CCD camera of a corroding surface to obtain maps of their coating by a corrosion/passivated layer.

Carbon steel in highly alkaline environment is a system of interest, it is protected from corrosion by the formation of a passive film with a thickness of few nm.[14] This passive film forms spontaneously in air, but its properties (thickness, composition, crystallinity) evolve in solution as a function of time and electrochemical potential, which can be tuned by a potentiostat for a laboratory study or controlled by the surrounding environment - as is the case of a free-corroding system. Ellipsometry measurements have previously shown that an oxide layer several nm thick grows linearly with increasing potential. X ray photo-electron spectroscopy (XPS) analyses have shown that the passive film was composed of mixed Fe(III) and Fe(II) oxides.[15] Although a passive film usually remains thin, its structure and properties may vary throughout it, making it difficult to obtain a fine description of its properties with a single experiment. In recent works, we showed that electrochemical impedance spectroscopy (EIS) provides a powerful approach to access thin-film properties.[16] Interestingly, it was shown that the use of an appropriate representation of the data (*i.e.* the Cole-Cole representation), allows extrapolation of parameters such as the high frequency capacitance, which can in turn allows the oxide film thickness to be determined.[17]

In this work, *in situ* electrochemical and light reflectivity microscopy were coupled to understand the electrochemical behavior of C15 mild steel in a 0.1 M NaOH reference solution at pH 13. Firstly, a global analysis was performed to compare electrochemical and reflectivity methods during passive film growth at bare steel, starting from the cathodic potential range. Then, surface reflectivity images were analyzed in order to obtain a dynamic measurement of the local transformation of the passive film during polarization.

2. Experimental

2.1. Materials

The working electrode consisted of a C15 mild-steel rebar commonly used as reinforcement in concrete, the composition of which was in agreement with EN 10277-2 norm. The lateral surface of the cylinder was first covered with an insulating cataphoretic paint (a few tens of micrometers) before being coated by an additional epoxy resin (few millimeters). The geometrical surface area exposed to the solution (corresponding to the cross section of the steel bar) was *c.a.* 0.38 cm^2. Before each experiment, the electrode was mechanically polished with SiC paper grade 2400, followed by diamond paste (1 μm), and then degreased in an ultrasonic bath for 1 minute in ethanol and 1 minute in distilled water. Electrochemistry was carried out in a classical three-electrode configuration using a reference electrode, the C15 steel as the working electrode, and a platinum counter electrode.

2.2. Methods

The electrochemical measurements were performed with a CH instrument potentiostat (IJ Cambria) in 0.1 M NaOH solution (pH = 13) using steady-state measurements (anodic and cathodic polarization curves) as well as EIS and chronoamperometry. EIS diagrams were performed at different polarization potentials as a function of time and were analyzed in order to evaluate the surface reactivity and the variation of the passive-layer thickness at the steel surface (*vide infra*).
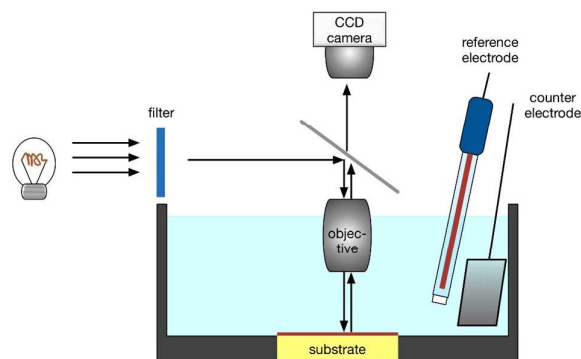
Fig. 1: Schematic representation of the experimental setup for performing the simultaneous measurement of the light reflectivity and the electrochemical response.

Additionally, the surface evolution during the electrode polarization (*i.e.* the formation or the removal of the passive layer) was investigated *in situ* and in real-time by light-reflectivity microscopy,[13b] which were performed with an in-house developed setup (Fig. 1). It consisted of a standard microscope (Olympus), equipped with a liquid immersion objective (Olympus UPlanFL) and a CCD camera (PhtotonFocus MV-D1024E-160-CL). The light source was a halogen white lamp, filtered at 490 nm with an interference filter (spectral bandwidth of 20 nm). The substrate was illuminated from the top by a blue light beam *via* the microscope objective. The reflected light was collected by the same objective and sent to the CCD camera, which allows real time imaging of the light flux reflected by the analyzed surface. Such a setup allowed 3D spatiotemporal imaging with a sub-micrometer lateral resolution (optical resolution) and sub-nanometer thickness sensitivity of the local passive film growth on the reflecting steel electrode. Before experiments, planarity of the surface domain to be analyzed was achieved using an interference Mirau objective and by minimizing the concentric interference fringes.[13b] All captured data were treated using in-house developed software under Matlab environment, which allows the calculation in reflectivity variation for different selected surface areas on the electrode.

3. Theory

3.1. Electrochemical impedance spectroscopy analysis

The high frequency time constant can be used to evaluate the capacitance of the electrode/solution interface. However, due to non-ideal behavior of electrochemical system, it usually results in frequency dispersion that is often described by a constant phase element (CPE). Such an element is useful for an electrical representation of the interface, but it hinders the physical meaning of the frequency dispersion observed experimentally.

The CPE impedance is expressed in terms of two model parameters α and Q as:

$$Z_{CPE}(\omega) = \frac{1}{Q(j\omega)^{\alpha}}$$ Eq. 1

when $\alpha = 1$, the parameter has units of a capacitance; otherwise, Q has units of $\Omega^{-1} cm^{-2} s^{\alpha}$ and $\omega = 2\pi f$.

These two CPE parameters can be graphically obtained following the method presented by Orazem *et al.*[18] The parameter α is calculated from the slope of the $\log|Z''|$ *vs* $\log f$ curve in the adequate frequency domain (*i.e.* in the frequency domain on which the CPE dominates the impedance response):

$$\alpha = \left| \frac{d\log|Z''(f)|}{d\log f} \right|$$ Eq. 2

and Q is readily calculated from α using the following relationship:

$$Q = -\frac{1}{Z''(f)(2\pi f)^{\alpha}} \times \sin\left(\frac{\alpha\pi}{2}\right)$$ Eq. 3

In the case of an oxide film formed at the electrode surface, the CPE behavior is generally attributed to a normal time constant distribution induced by a significant variation of resistivity within the film. It was shown that in this case, the power-law model can properly describe in a proper way the CPE behavior.[19]

In addition, since a CPE element is equivalent to a ladder of Voigt's elements in series,[19] the extrapolation of the Cole-Cole diagram at infinite frequency can be a reliable way to determine the thickness of the oxide layer[20] according to the following formula[16b]

$$\delta_{ox} = \frac{\varepsilon \varepsilon_0}{C_{ox}}$$

Eq.4

where ε_0 is the permittivity of vacuum ($\varepsilon_0 = 8.85 \; 10^{-14}$ Fcm^{-1}) and $\varepsilon = 12$ (dielectric constant for Fe_2O_3 assuming that the passive layer consisted of a pure iron oxide, only). Indeed, the Cole-Cole representation consisted of a capacitance spectrum plotted using the impedance spectrum corrected from the electrolyte resistance R_e according to:

$$C(\omega) = \frac{1}{j\omega \left[Z(\omega) - R_e \right]}$$

Eq.5

The oxide film capacitance extrapolated in the high frequency domain and the use of Eq. 4 thus provides an estimate of the layer thickness, and from the values of the CPE parameters, Q and α, the resistivity profile within the oxide film can be calculated.[17]

3.2. Light reflectivity

In the case of a normal incidence, the light reflectivity, R, of an electromagnetic wave propagating in a medium **A** (characterized by its real index n_A) reflecting on a substrate, **S**, (characterized by its complex refractive index $\tilde{n}_S = n_S + i \cdot k_S$) is the square of the modulus of the reflection coefficient and is given by the Eq. 6:

$$R = \left| \tilde{r}_{AS} \right|^2 = \left| \frac{n_A - \tilde{n}_S}{n_A + \tilde{n}_S} \right|^2$$

Eq. 6

When an intermediate thin film of thickness δ and characterized by a refractive index n_F, is intercalated between the substrate and the medium (such as a passive layer which is sandwiched between the steel electrode and the electrolytic solution), the expression of the

light reflectivity can be expressed as:

$$R = \left| \frac{\tilde{r}_{AF} + \tilde{r}_{FS}\, e^{2i\frac{2\pi}{\lambda}n_F\delta}}{1 + \tilde{r}_{AF}\tilde{r}_{FS}\, e^{2i\frac{2\pi}{\lambda}n_F\delta}} \right|^2$$

Eq. 7

where λ is the wavelength of the incident beam, and $\tilde{r}_{AF}$ and $\tilde{r}_{FS}$ are the complex reflection coefficients at medium A / thin film, and thin film / substrate interfaces, respectively. Assuming the incident light intensity remains constant throughout the experiment, the variation of the reflected light intensity can be measured at different time t compared to the reflected light intensity recorded at $t = 0$.[13b] The relative variation of the reflectivity, $\dfrac{\Delta R}{R}$, is then linked to the reflected beam intensity through the following relationship:

$$\frac{I_{reflect}(t)}{I_{reflect}(0)} = 1 + \frac{\Delta R}{R}$$
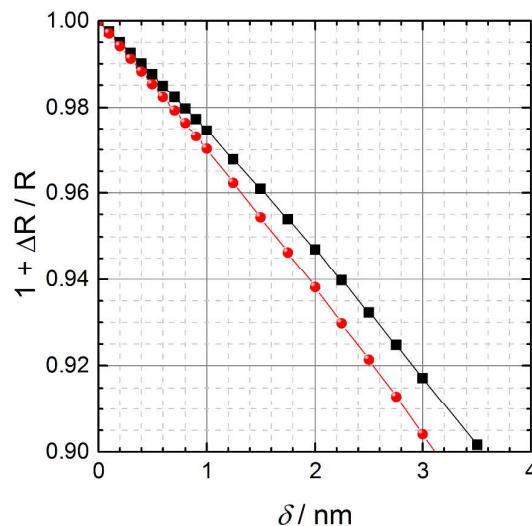
Eq. 8

Fig. 2: Calculated reflectivity as a function of the oxide layer thickness using Eq. 7 for steel/hematite/water (red circles) and steel/hematite/air (black squares) for $\lambda = 490$ nm,

$$n_F^{Fe} = 2.72,\ k^{Fe} = 2.86,\ n_F^{Fe2O3} = 2.92,\ n_F^{air} = 1,\ n_F^{Water} = 1.33$$

Fig. 2 illustrates the variations in relative reflectivity calculated with Eq. 7 for steel / Fe_2O_3(hematite) / air (red circles) and steel / Fe_2O_3(hematite) / water (black squares) systems. The assumption is made that the layer formed at the steel surface is pure iron oxide, which is in fair agreement with the nominal composition of steel used in this work, and that the oxide is pure hematite (refractive index is n_F = 2.92). In the case of a layer made of magnetite (Fe_3O_4), a n_F value of 2.42 has to be taken into account,[21] but the same linear variation is observed. Note, the accessible domain shown here (between 3 and 4 nm for a 10 % of relative reflectivity variation for Fe_2O_3) is fully compatible with the characteristic dimensions usually encountered for a passive layer on steel in NaOH solution.[22] Additionally, the relationship between thickness and relative reflectivity is almost linear in this domain, a 1% variation in the relative reflectivity corresponds to a variation of about 0.35 nm for the thickness of Fe_2O_3, while it corresponds to a 0.2 nm thickness for the less refractive Fe_3O_4 oxide. Hence, the reflectivity method allows accurate monitoring of the early stages of passive film transformation.

4. Results and discussion

4.1. The early stage of the formation of a passive layer on a bare steel surface.

Electrochemical and surface reflectivity measurements were first compared for the electrochemical growth of an oxide layer on a bare steel surface, assuming that the oxide layer is mainly made of Fe_2O_3.

4.1.1. Potentiostatic measurements in the cathodic domain

The steady-state cathodic polarization curve in Fig. 3 was obtained in 0.1 M NaOH solution starting from -1.80 V/MSE, where the air-formed native oxide is assumed to be reduced, towards a potential close to *E_{corr} (about -0.55 V/MSE)* by successive steps of 50 mV. We

assumed that a steady-state behavior was reached for each polarization potential when the corresponding current variations were smaller than 0.4 $\mu A/cm^2$ for 2 min.
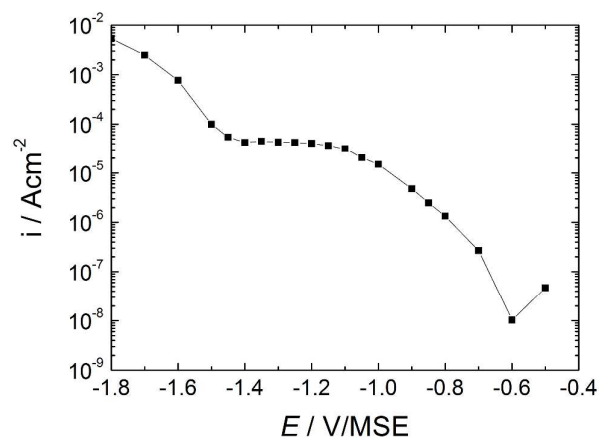
Fig. 3: *Steady-state polarization curve (cathodic domain) of C15 mild steel in 0.1 M NaOH*

The curve shows a current plateau between -1.5 and -1.2 V/MSE usually attributed to dissolved oxygen reduction with a total transfer of 4 electrons as

$$O_2 + 2\,H_2O + 4\,e^- \rightleftharpoons 4\,OH^-$$ Eq. 9

It should be mentioned that the boundaries of this potential window might vary by a few tens of mV from one experiment to the other. In this domain, the reaction is limited by mass transport only. For less negative potentials, the current decreases with increasing potential, indicating that oxygen reduction is controlled simultaneously by diffusion and charge transfer (mixed control). Simultaneously, an oxide film grows, but no feature corresponding to iron oxidation is observed in the potentiodynamic curve. The overall cathodic current is the sum of the current due to oxygen reduction on a bare metallic, or on a partially oxidized surface, and of an anodic current due to oxide formation. The increase in current at potentials negative to *E*=-1.5 V/MSE was ascribed to water reduction with the production of H_2 simultaneously with the oxygen reduction reaction (ORR). This potential domain was not investigated in this

work since a gas evolving reaction is not compatible with further reflectometry measurements.

4.1.2. Electrochemical impedance spectroscopy (EIS) measurements

EIS measurements were obtained after several minutes of immersion in static conditions to ensure a steady-state behavior, scanning from a more cathodic potential to a potential close to E_{corr} (Fig. 4). Each measurement shows a capacitive behavior, the diameter of the capacitive loop being large for potentials close to $E_{corr} \sim$ -0.55 V/MSE. The loop diameter decreases with decreasing potential until E=-0.90 V/MSE and then increases for potential negative to E=-1.15 V/MSE (corresponding to the beginning of the oxygen reduction plateau). A fine examination of the EIS diagrams shows that the semi-circles are flattened, and can be described by a CPE behavior as previously discussed. These impedance results combined with the steady-state polarization curves allow us to define three domains in the reduction reaction of dissolved oxygen:

- Between E_{corr} and E=-0.90 V/MSE, the shape of the impedance diagrams and the low frequency limit are characteristic of the presence of an oxide layer formed on the steel surface. Therefore, the ORR takes place on an oxidized surface and is mainly limited by charge transfer. In fact Vago et *al.*[23], showed that the reduction of O_2 on an oxide layer occurs simultaneously with the electrochemical reduction of the oxidized surface, whereas Calvo et *al.*[24] showed that the reduction of oxygen on passive iron in alkaline solution occurs only in the potential range where the passive film is partly reduced.

- For potential between E=-0.95 and E=-1.15 V/MSE, the diameter of the capacitive loop slightly increases when the applied potential decreases. In this case, the ORR takes place on a partially bare steel surface and the reaction is under mixed control.
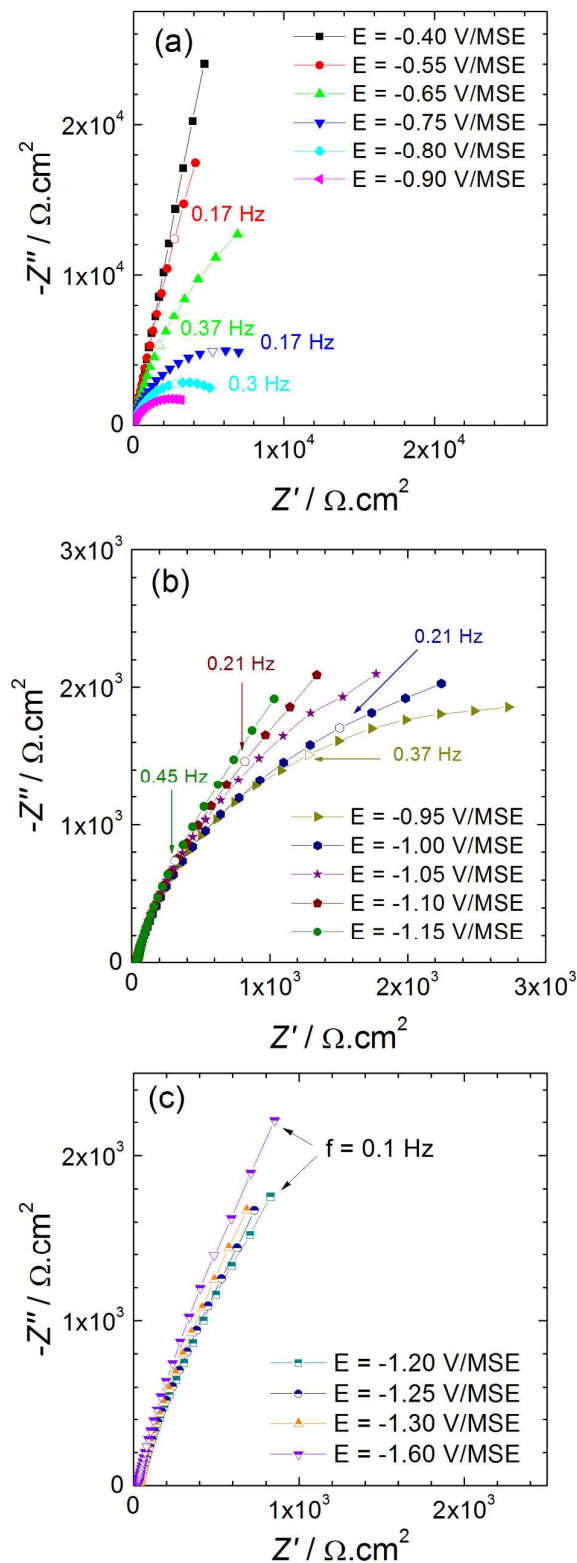
Fig. 4: *Impedance diagrams obtained for C15 mild steel in 0.1 M NaOH solution at different cathodic potentials.*

- For more cathodic potential, between $E=$ -1.15 and $E=$-1.5 V/MSE, the shape of the impedance diagram remains unchanged whereas the polarization curves shows that in this domain the ORR is diffusion controlled. For a more negative potential (e.g. -1.6 V/MSE), both ORR and water reduction simultaneously occur on the electrode.

The capacitance of the oxide layers was determined using the Cole-Cole representation (as exemplified in Fig. 5 for $E=$-1.2 V/MSE) for the cathodic potential measurements. The capacitance value obtained as the high-frequency limit of the real part of the capacitive plot was then used to calculate the oxide layer thickness from Eq. 4. δ_{ox} varies from 1 nm for $E=$-1.25 V/MSE to 3 nm for –0.4 V/MSE (Table 1), which is in good agreement with usual values encountered in the literature.
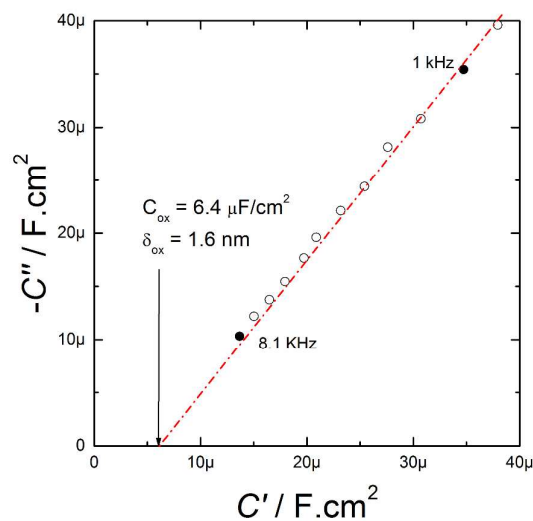
Fig. 5: *Cole-Cole diagram obtained at -1.2 V/MSE*

Table 1: *Capacitance and oxide thickness obtained from the Cole-Cole plot*

E (V/MSE)	C_{ox} (F/cm^2)	δ_{ox} (nm)
-0.400	3.0×10^{-6}	3.2
-0.550	4.0×10^{-6}	2.4
-0.650	3.8×10^{-6}	2.5
-0.750	4.6×10^{-6}	2.1
-0.800	4.8×10^{-6}	2.0
-0.900	5.1×10^{-6}	1.9
-0.950	5.4×10^{-6}	1.8
-1.000	5.3×10^{-6}	1.8

-1.050	6.3×10^{-6}	1.6
-1.150	5.6×10^{-6}	1.7
-1.200	6.4×10^{-6}	1.5
-1.250	6.4×10^{-6}	1.5

Independent determination of δ_{ox} values is very useful, since it can in turn be used in the model for analyzing the EIS diagrams, e.g. in determining the resistivity profile inside the thin film.[25] In the potential range negative to -1.25 V/MSE, the Cole-Cole representation shows a pure CPE behavior indicating that the cathodic reaction takes place on a bare surface. In this case, the origin of the CPE is ascribed to a surface distribution of time constant involving both the charge transfer resistance, R_{ct}, and the double layer capacitance, C_{dl}, which can be evaluated with the Brug's relationship[16a]

$$C_{dl} = Q^{1/\alpha} \left(\frac{1}{R_e} + \frac{1}{R_{ct}} \right)^{(\alpha-1)/\alpha} \qquad \text{Eq. 10}$$

4.1.3 Reflectivity measurements in the cathodic range

The surface reflectivity was measured during a linear potential sweep from E=-1.15 V/MSE to E=-0.6 V/MSE at $v = 1$ mV/s (Fig.6a). This figure shows the variations of surface reflectivity for four different domains with surface areas of 30 μm^2 (left scale), simultaneously with the total current of the electrode (right scale). All the curves are very similar and show the same trends and boundary limits, indicating that the film formation is homogeneous over electrode surface. The scan rate of $v = 1$ mV/s was a good compromise between the need of reaching a quasi-steady-state regime for electrochemical measurement and the rate of image acquisition of the set-up (1 picture each 2 seconds).
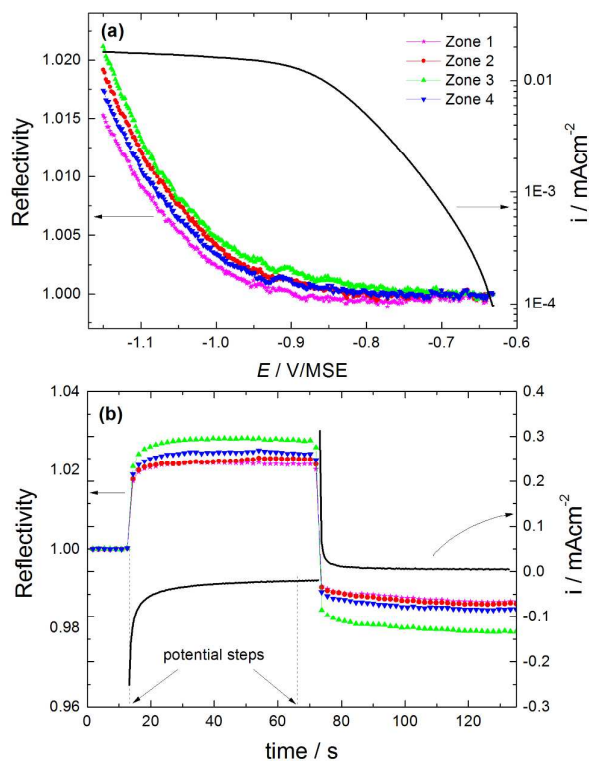
Fig. 6: *Surface reflectivity measurement performed on C15 mild steel in 0.1 M NaOH solution during a linear variation of the potential at v = 1 mV/s and simultaneous measurement of the current (a), and for two successive potential steps from E$_{corr}$ to E=-1.5 V/MSE and then to E=-0.87 V/MSE (b)*

The oxide film growth/dissolution was also investigated by performing potential step experiments at two different potentials in the cathodic range and by measuring simultaneously the current and reflectivity variations. First, the corrosion potential was measured for 10 seconds, and then two potential steps were successively applied at -1.5 V/MSE, where the oxygen diffusion plateaus, and the second at - 0.87 V/MSE, in the vicinity of E$_{corr}$. At the same time surface images were recorded every 2 seconds (Fig. 6b). After the first potential step, a cathodic current transient is observed corresponding to the reduction of the passive film previously formed at the corrosion potential. The time constant of this transient is about 10 seconds and then the current decreases slowly reaching a steady state value after 70 seconds. The relative reflectivity variations for 4 different domains (about 100x100 μm^2 each) above the electrode surface are also reported (left scale). On each domain, an increase in the

reflectivity, by 2 to 3 % of the initial value, was observed which is ascribable, as previously, to the reduction of the passive film formed at the corrosion potential. Interestingly, the time constant associated with this phenomenon is similar to the value obtained from the current analysis as a function of time. In addition, the calibration curve relative to Fe_2O_3 (Fig. 2) allowed estimation of the film thickness variation between 0.85 and 1.05 nm. After about 75 seconds, the potential was stepped to a more anodic value leading to an anodic current transient ascribed to a passive film formation. The surface reflectivity at this potential was smaller than the initial value by about 1.5 – 2 %, corresponding to a thickness between 0.5 and 0.85 nm. From these two successive experiments, an overall reflectivity variation in the range of about 4% was obtained, allowing the *in situ* evaluation of the film thickness to be about 1.5 to 2 nm after 70 seconds of polarization at -0.87 V. This is in good agreement with the results obtained by EIS (Table 1). The variation in the surface reflectivity also indicates that the film thickness changes within a short time-scale, as a bare surface was obtained after 15 to 20 seconds of electrode polarization on the oxygen reduction plateau. The formation of the passive film was achieved in the same time-scale, although it is well established that its structure may evolve as a function of time.[26] Similar measurements were performed at different cathodic potentials in order to evaluate the evolution of the oxide film thickness as a function of the potential. Interestingly, it was shown that a bare metallic surface is present at potentials negative to -1.5 V, and that the oxide layer grows between -1.5V and -1.3 V. Then the film thickness is roughly constant over a wide cathodic domain after 70s of polarization.

Thus, both electrochemical and reflectometry measurements provide similar estimations of the oxide layer thickness in the investigated potential range, validating the use of both techniques for measuring *in situ* the thickness of the oxide layer. This is an important result as it offers the possibility to obtain the film thickness whatever the model used for fitting the EIS response of the system.

1
2
3
4
5
6
7
8
9
10
11
12
13
14
15
16
17
18
19
20
21
22
23
24
25
26
27
28
29
30
31
32
33
34
35
36
37
38
39
40
41
42
43
44
45
46
47
48
49
50
51
52
53
54
55
56
57
58
59
60

4.2. Modification in the passive layer during cathodic and anodic polarization.

Corrosion layers on carbon steel in an alkaline medium are generally much more complex than a simple Fe_2O_3 layer. Fig. 7 shows successive cyclic voltammograms (CVs) of the C15 steel simultaneously with the reflectivity monitoring. During the first cycle (Fig. 7a), the forward cathodic scan from -0.45 V/MSE to -1.45 V/MSE, shows a cathodic current due to oxygen reduction. The reflectivity variations confirm that O_2 reduction is accompanied at more cathodic potentials by the reductive thinning of the passive film. On the backward anodic scan, the passive film regrows. The insert in the first cycle of Fig. 7a compares the anodic charge estimated from the backward scan with the variation of the apparent film thickness estimated from the reflectivity, assuming that Fe_2O_3 is the main component in the passive layer. A roughly linear variation is observed between the anodic charge and the thickness of the layer with a proportionality factor of about 0.2 nm cm^2/mC.

The formation of Fe_2O_3 by iron oxidation through Eq. 11 would account for a proportionality factor of 0.52 nm cm^2/mC, suggesting that the reaction proceeds with a 38% efficiency.

$$2 \text{ Fe} + 6 \text{ HO}^- \rightarrow Fe_2O_3 + 3 \text{ H}_2O + 6 \text{ e}^- \qquad \qquad \text{Eq. 11}$$
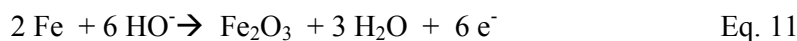
Following the first cycle, the electrodes reflectivity is slightly less than its initial, suggesting the surface does not revert to its original state following the CV with a thicker oxide layer formed. Similar effect was previously monitored by in situ UV absorption.[10a] It was suggested that the oxidation/reduction in NaOH does not reversibly grow and thin out the passive film, with recovery of the metallic Fe surface at the most cathodic potentials, but rather that a porous Fe (II) deposit/precipitate is formed during cathodic polarization. Then, upon backward anodic polarization, the passive film can regrow between the Fe(0) and the Fe(II) deposit, the Fe(II) deposit being further oxidized into a precipitate layer of Fe(III) oxide according to

$$3 \text{ Fe}_2O_3 + 2 \text{ e}^- + \text{H}_2O \Leftrightarrow 2 \text{ Fe}_3O_4 + 2 \text{ HO}^- \qquad \qquad \text{Eq. 12}$$
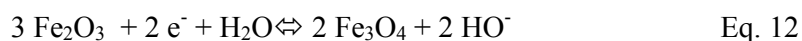
The Fe(III)/Fe(II) oxide materials conversion is confirmed by the appearance of new electrochemical features upon subsequent cycles (Fig. 7b); the anodic and cathodic peaks at -1.05 and -1.4 V/MSE, respectively. The evolution of the light reflectivity as a function of the electrode potential considerably changed with two sharp reflectivity variations now detected simultaneously with the two new peaks. The reflectivity variation associated with the forward reduction of Fe(III) into Fe(II) oxide at -1.4 V is smaller than that associated to the reverse reaction at -1.05 V on the backward scan, confirming that the process at hand is not reversible during the potential cycle, at least in the potential domain investigated in this work.
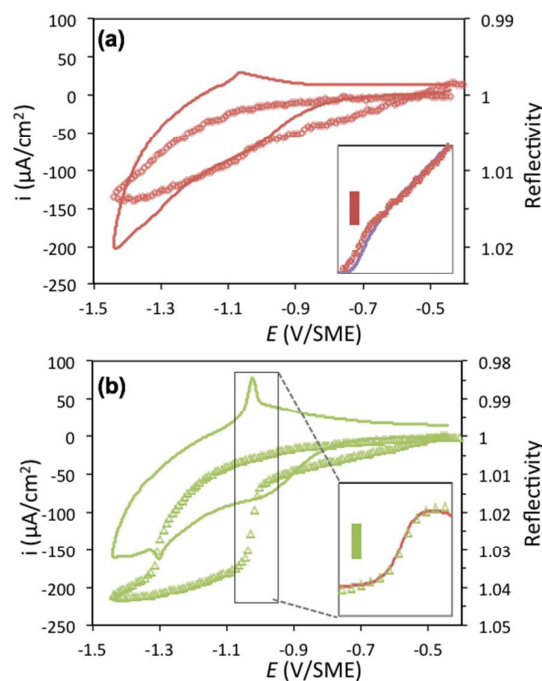
Fig.7: *First (a) and second (b) cyclic voltammograms (lines) of a C15 steel electrode recorded at 5mV/s (from -0.45 $\rightarrow$ -1.45 $\rightarrow$ -0.45 V), simultaneously with reflectivity (symbols) averaged over a 100x100 μm^2 electrode surface area. Inserts: variation of the anodic charge and (a) thickness of deposited passive film during the backward potential scan (-1.1 $\rightarrow$ -0.45V) for the first cycle, or (b) reflectivity change during the anodic peak at -1.05 V on the second cycle; the vertical bar corresponds to (a) 0.5mC/cm^2 and 0.1 nm of apparent thickness or (b) 0.12mC/cm^2 and 1% change in reflectivity.*

Considering the molecular volume of Fe_2O_3 and Fe_3O_4, the phase transformation formalized by reaction 12 leads to an estimate of a change in film thickness lower than 2%, The large

change in reflectivity detected during the cycling transformation is then mainly due to the

change in refractive index of both materials from $n_F = 2.92$ for Fe_2O_3 to $n_F = 2.42$ for Fe_3O_4.

Qualitatively, the reduction (resp. oxidation) is accompanied with an increase (resp. decrease)

of reflectivity in agreement with the transformation of the coating into a less (resp. more)

refractive material (Fe_3O_4, resp. Fe_2O_3). Quantitatively, the insert of Fig. 7b shows a good

correlation between the reflectivity variation and the charge exchanged along the anodic peak.

Based on the changes of the values of n_F, the measured reflectivity change during the anodic

peak would correspond to the transformation of a 1.3 nm thin film of Fe_3O_4 while the

integration of the anodic peak corresponds to an exchange of 0.25 mC/cm^2 charge density,

yielding a molecular volume of transformed material of ca. 50.2 cm^3/mol, in good agreement

with the expected value of 44.7 cm^3/mol for Fe_3O_4.

4.3. From reflectivity images to local reactivity images

It is difficult to probe the heterogeneity of the steel surface with scanning electrochemical

probe microscopies. Indeed, we were unable to demonstrate these variations using local

electrochemical measurements and, in particular, local electrochemical impedance[27] due to

the time-scale of the interface evolution - observable only within the first moments of the

passive film formation and therefore not compatible with the time scale of electrochemical

mapping techniques.

However, one can take advantage of the spatial information provided by reflectivity images as

each image pixel contains chemical information, i.e. the local amount of iron oxide coating,

and each surface image can be recast into an image of local relative thickness of iron oxide.

Fig.8a is a 60x60 μm^2 sample of the image of the electrode before its polarization. Apart from

polishing lines or inclusions (black dots), the surface is quite heterogeneous and is speckled

with micrometric islands that are regions of lower reflectivity than the surrounding surface.

The electrode was scanned cathodically (CV curve - Fig.7a) whilst recording successive images of the electrode surface. Two examples of reflectivity changes on the same electrode domain are given in Figs. 8c and d, when the overall reflectivity is minimal (E=-1.4V/MSE backward scan of see Fig.7a) or at the end of the cycle (E=-0.45V/MSE, end of backward scan). If the stripes are still visible in these maps, the overall electrode is becoming more reflective in the cathodic domain and less reflective in the anodic domain, in agreement with the mechanisms proposed earlier[10a] for the growth/thinning of the oxide layer.

Typically, in Fig. 8a the brightest region is ca. 3% more reflective than the grey speckles, suggesting the image probes regions having difference in relative Fe_2O_3 coating thickness of the order of 1 nm. It is then possible to monitor the local kinetic of the transformation of the passive film. Under cathodic conditions (Fig. 8c), the most reactive regions are the dark speckles originally detected, which shows a higher extent of oxide reduction. It agrees with the first image suggesting that these dark speckles are originally coated with larger amount of oxide. Additionally, at the end of the CV, for an anodic potential (Fig. 8d), the same dark speckles are the most reactive regions and are now even darker than before the electrode polarization. While their surrounding regions return approximately to their original state, the dark speckles are now coated with a thicker, by ca. 0.2-0.3 nm, layer of oxide.

Fig. 8b presents the local reflectivity variations of two representative areas (2×2 μm^2) of dark and bright domains during the CV. The brightest regions present a quasi-reversible passive layer formation as usually observed in less alkaline conditions. On the other hand, a sharp and large reflectivity decrease is detected at the dark region site, suggesting a mechanism of progressive oxide deposition/precipitation during the transformation of the passive film. This was further confirmed from the inspection of the local behavior of the electrode during a second cycle, where the progressive coating with Fe_2O_3 of the darkest regions was also clearly

visualized, while the brightest regions seem to return to present a more reversible transformation upon cycling.
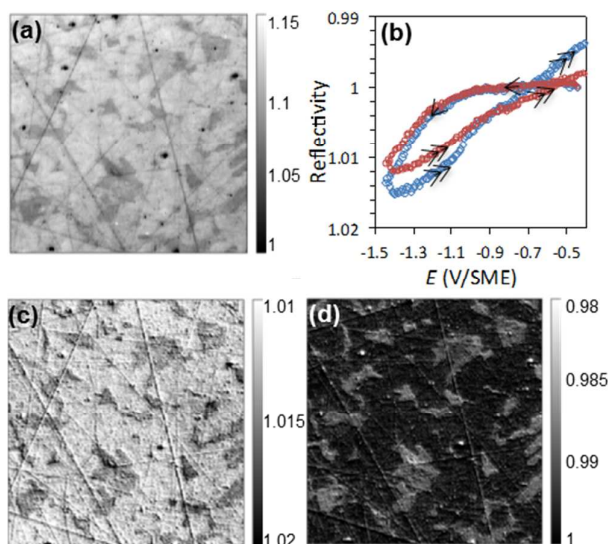
Fig. 8: Image of a steel surface immersed in 0.1 M NaOH at open circuit potential (a) and during a cyclic voltammogram on the reverse anodic scan at -1.4 V (c) or -0.45 V (d). (b) Local variation of reflectivity during voltammetry on 2x2μm areas corresponding to bright (red) or dark (blue) regions in (a). Apart from defects such as inclusions or strays, the darkest speckles representative of regions covered with thicker layers of iron oxide are clearly visible and showing higher activity.

5. Conclusions

We have successfully shown that we were able to monitor *in situ* the evolution of a passive film and determine a file thickness in the nm range as a function of time and applied potential using electrochemical methods coupled to surface reflectivity measurements. Transient analysis of the passivation process can be followed *in situ* and under polarization. The coupled optical and electrochemical analysis confirms that if a Fe_2O_3 passive layer can be formed upon oxidation, the reduction of this layer, in alkaline medium, tends to produce a Fe_3O_4 film. Due to its conductivity, this layer is likely difficult to detect from the single impedance spectroscopy measurement which would rather probe the presence of the passive Fe_2O_3 film.

This work further shows that the steel surface is heterogeneous and presents micrometric islands coated with thicker oxide layer than the surrounding surface. The monitoring of their local reflectivity change during successive cathodic and anodic polarization suggests that those regions are the more reactive and the more prone to the development and oxidation of the Fe_3O_4 porous layer, while the surrounding surface is more subject to a reversible passivation process.

Such images thus allowed the mapping of both the local thickness and the reactivity of the oxide layer during its formation and reduction, in other words it can be seen as an indirect impedance measurement, in which faradaic processes are frozen and the electrolyte resistance is disregarded.

References

1.   Albery, W. J.; Ulstrup, J., *Electrochim. Acta* **1968,** *13* (2), 281-284.
2.   Amatore, C.; Saveant, J. M.; Tessier, D., *J. Electroanal. Chem.* **1983,** *147* (1-2), 39-51.
3.   (a) Bard, A. J.; Denuault, G.; Lee, C.; Mandler, D.; Wipf, D. O., *Acc.Chem.Res.* **1990,** *23* (11), 357-363; (b) Mirkin, M. V.; Nogala, W.; Velmurugan, J.; Wang, Y., *Phys. Chem. Chem. Phys.* **2011,** *13*, 21196-21212; (c) Wittstock, G.; Burchardt, M.; Pust, S. E.; Shen, Y.; Zhao, C., *Angew. Chem. Int. Ed.* **2007,** *46* (10), 1584-1617.
4.   (a) Basame, S. B.; White, H. S., *Anal. Chem.* **1999,** *71* (15), 3166-3170; (b) Maho, A.; Kanoufi, F.; Combellas, C.; Delhalle, J.; Mekhalif, Z., *Electrochim. Acta* **2014,** *116*, 78-88.
5.   Casillas, N.; Charlebois, S. J.; Smyrl, W. H.; White, H. S., *J. Electrochem. Soc.* **1993,** *140* (9), L142-L145.
6.   Galicia, G.; Pebere, N.; Tribollet, B.; Vivier, V., *Corros. Sci.* **2009,** *51* (8), 1789-1794.
7.   (a) Eckhard, K.; Etienne, M.; Schulte, A.; Schuhmann, W., *Electrochemistry Communications*
 2007, *9* (7), 1793-1797; (b) Gabrielli, C.; Ostermann, E.; Perrot, H.; Vivier, V.; Beitone, L.; Mace, C., *Electrochem. Commun.* **2005,** *7* (9), 962-968; (c) Bandarenka, A. S.; Eckhard, K.; Maljusch, A.; Schuhmann, W., *Anal Chem* **2013,** *85* (4), 2443-8.
8.   (a) Patel, A. N.; Collignon, M. G.; O'Connell, M. A.; Hung, W. O.; McKelvey, K.; Macpherson, J. V.; Unwin, P. R., *J Am Chem Soc* **2012,** *134* (49), 20117-30; (b) Chen, C. H.; Meadows, K. E.; Cuharuc, A.; Lai, S. C.; Unwin, P. R., *Phys Chem Chem Phys* **2014,** *16* (34), 18545-52.
9.   Lu, Z. J.; Macdonald, D. D., *Electrochim. Acta* **2008,** *53* (26), 7696-7702.
10.   (a) Buchler, M.; Schmuki, P.; Bohni, H., *J. Electrochem. Soc.* **1997,** *144* (7), 2307-2312; (b) Buchler, M.; Schmuki, P.; Bohni, H., *J. Electrochem. Soc.* **1998,** *145* (2), 609-614.
11.   Schmuki, P.; Buchler, M.; Virtanen, S.; Bohni, H.; Muller, R.; Gauckler, L. J., *J. Electrochem. Soc.* **1995,** *142* (10), 3336-3342.
12.   (a) Shan, X. N.; Patel, U.; Wang, S. P.; Iglesias, R.; Tao, N. J., *Science* **2010,** *327* (5971), 1363-1366; (b) Wang, W.; Foley, K.; Shan, X.; Wang, S.; Eaton, S.; Nagaraj, V. J.; Wiktor, P.; Patel, U.; Tao, N., *Nat Chem* **2011,** *3* (3), 249-55.
13.   (a) Munteanu, S.; Garraud, N.; Roger, J. P.; Amiot, F.; Shi, J.; Chen, Y.; Combellas, C.; Kanoufi, F., *Anal Chem* **2013,** *85* (4), 1965-71; (b) Munteanu, S.; Roger, J. P.; Fedala, Y.; Amiot, F.; Combellas, C.; Tessier, G.; Kanoufi, F., *Faraday Discussions* **2013,** *164*, 241.
14.   Ghods, P.; Isgor, O. B.; Bensebaa, F.; Kingston, D., *Corros. Sci.* **2012,** *58*, 159-167.
15.   (a) Ohtsuka, T.; Azumi, K.; Sato, N., *Passivity of Metals and Semiconductors.* 1983; (b) Sato, N.; Noda, T.; Kudo, K., *Electrochim. Acta* **1974,** *19* (8), 471-475; (c) Ohtsuka, T.; Azumi, K.; Sato, N., *Corros. Sci.* **1990,** *31*, 155-160; (d) Sato, N.; Noda, T., *Electrochim. Acta* **1977,** *22*, 839.
16.   (a) Hirschorn, B.; Orazem, M. E.; Tribollet, B.; Vivier, V.; Frateur, I.; Musiani, M., *Electrochim. Acta* **2010,** *55* (21), 6218-6227; (b) Hirschorn, B.; Orazem, M. E.; Tribollet, B.; Vivier, V.; Frateur, I.; Musiani, M., *J. Electrochem. Soc.* **2010,** *157* (12), C458-C463.
17.   Benoit, M.; Bataillon, C.; Gwinner, B.; Miserque, F.; Orazem, M. E.; Sánchez-Sánchez, C. M.; Tribollet, B.; Vivier, V., *Electrochim. Acta* **2016,** *201*, 340-347.
18.   Orazem, M. E.; Pébère, N.; Tribollet, B., *J. Electrochem. Soc.* **2006,** *153* (4), B129-B136.
19.   Hirschorn, B.; Orazem, M. E.; Tribollet, B.; Vivier, V.; Frateur, I.; Musiani, M., *J. Electrochem. Soc.* **2010,** *157* (12), C452-C457.
20.   Jonscher, A. K., *Electrochim. Acta* **1990,** *35* (10), 1595-1600.

21.   Batsanov, S. S.; Ruchkin, E. D.; Poroshina, I. A., In *Refractive Indices of Solids*, Springer Singapore: Singapore, 2016; pp 1-108.

22.   Abd El Haleem, S. M.; Abd El Aal, E. E.; Abd El Wanees, S.; Diab, A., *Corros. Sci.* **2010,** *52* (12), 3875-3882.

23.   Vago, E. R.; Calvo, E. J., *J. Electroanal. Chem.* **1992,** *339* (1-2), 41-67.

24.   Calvo, E. J.; Schiffrin, D. J., *J. Electroanal. Chem.* **1988,** *243* (1), 171-185.

25.   Orazem, M. E.; Frateur, I.; Tribollet, B.; Vivier, V.; Marcelin, S.; Pebere, N.; Bunge, A. L.; White, E. A.; Riemer, D. P.; Musiani, M., *J. Electrochem. Soc.* **2013,** *160* (6), C215-C225.

26.   (a) Diezperez, I.; Sanz, F.; Gorostiza, P., *Current Opinion in Solid State and Materials Science* **2006,** *10* (3-4), 144-152; (b) Massoud, T.; Maurice, V.; Klein, L. H.; Marcus, P., *J. Electrochem. Soc.* **2013,** *160* (6), C232-C238.

27.   (a) Lillard, R. S.; Moran, P. J.; Isaacs, H. S., *J. Electrochem. Soc.* **1992,** *139* (4), 1007-1012; (b) Huang, V. M.-W.; Wu, S.-L.; Orazem, M. E.; Pebere, N.; Tribollet, B.; Vivier, V., *Electrochim. Acta* **2011,** *56*, 8048-8057.